Extracting W boson couplings from the e^+e^- production of four leptons

Pat Kalyniak, Paul Madsen, and Nita Sinha
Ottawa-Carleton Institute for Physics, Physics Department, Carleton University, 1125 Colonel By Drive, Ottawa, Canada K1S 5B6

Rahul Sinha
Theoretical Physics Group, Tata Institute of Fundamental Research, Homi Bhabha Road, Bombay 400 005, India
(Received 30 March 1993; revised manuscript received 11 August 1993)

We consider the processes $e^+e^- \to \ell^+\ell'^-\nu\bar{\nu}'$, including all the possible charged lepton combinations, with regard to measuring parameters characterizing the W boson. These reactions all proceed via virtual W pair production as well as a number of undistinguished s- and t-channel modes. In addition, some of the processes also have contributions from other diagrams of interest, those which contain the γWW or ZWW vertices with gauge bosons in the t channel. Consequently, the processes are sensitive to anomalous couplings such as κ_γ and κ_Z. We here calculate at what level these processes can be used to measure these anomalous couplings for the cases of e^+e^- colliders at 500 GeV and 1 TeV center-of-mass energies. Further, we present helicity information which should be useful in distinguishing between deviations of κ_γ from its standard model value and deviations of κ_Z.

PACS number(s): 13.10.+q, 14.80.Er

I. INTRODUCTION

The gauge boson couplings of the standard model of electroweak interactions are only just beginning to be directly measured. There has now been observation of the process $p\bar{p} \to e\nu\gamma X$, presumably representing $W\gamma$ production and radiative W decay, at the Collider Detector at Fermilab (CDF) [1] and at UA2 at CERN [2]. In principle, indirect evidence regarding the gauge boson couplings comes from higher order corrections to low energy measurements. However, it appears that the sensitivity to such loop-induced effects of the trilinear gauge boson interaction has been overestimated in much of the literature [3,4]. There now exists some preliminary work on a global analysis of low energy data and data from the CERN e^+e^- collider LEP, in order to extract bounds on the gauge boson couplings [3,5]; the present results are model dependent and incomplete and should be refined.

The prospect of increasing accumulated luminosity at existing facilities and of future facilities encourages detailed work on the means of constraining the gauge boson couplings. We focus here on the possibility of measuring parameters relevant to the γWW and ZWW vertices. The couplings of W bosons to the photon and Z can be described in general by an effective Lagrangian with seven parameters for each of the neutral gauge bosons [6,7]. We will here neglect CP-violating parameters as they are constrained to be less than $\sim 10^{-4}$ by neutron electric dipole moment measurements [8]. An effective Lagrangian respecting CP, C, and P invariance is often parametrized as

$$L = -ig_V\left(g_1^V(W^\dagger_{\mu\nu}W^\mu - W^{\dagger\mu}W_{\mu\nu})V^\nu + \kappa_V W^\dagger_\mu W_\nu V^{\mu\nu} + \frac{\lambda_V}{M_W^2}W^\dagger_{\lambda\mu}W^\mu_\nu V^{\nu\lambda}\right). \quad (1.1)$$

In the above equation, V represents either the photon or the Z boson and the overall couplings are taken as $g_\gamma = e$ and $g_Z = e\cot\theta_W$. The parameters κ_γ and λ_γ are related to the static magnetic dipole and electric quadrupole moments μ_W and Q_W, respectively, of the W boson as follows:

$$\mu_W = \frac{e}{2M_W}(1+\kappa_\gamma+\lambda_\gamma),$$
$$Q_W = -\frac{e}{2M_W}(\kappa_\gamma-\lambda_\gamma).$$

The tree level standard model values of the parameters of Eq. (1.1) are $g_1^V = 1$, $\kappa_V = 1$, and $\lambda_V = 0$. If the W bosons are composite objects, then deviation of the triple gauge boson coupling parameters from their standard model values could be very large indeed; as an example, κ has been calculated to be greater than 3 in one model [9]. However, within the standard model, upper bounds on the one-loop corrections to the tree level values of κ_γ and λ_γ have been given as [10]

$$(\Delta\kappa_\gamma)_{\max} = 1.5\%,$$
$$(\Delta\lambda_\gamma)_{\max} = 0.25\%.$$

In extensions of the standard model such as those containing extra Higgs doublets, extra heavy fermions [10], or supersymmetric (SUSY) extensions [11] the deviations from the tree level standard model values tend to be of about the same order of magnitude as these one-loop corrections. Also, $\Delta\lambda$ is usually (although not always) smaller than $\Delta\kappa$ by close to an order of magnitude, bringing it below 1%. Hence we will here neglect deviations of λ from its standard model value of zero and will present numerical results where κ_γ and κ_Z vary only within 10% of 1.

We investigate a set of processes of four lepton production in e^+e^- collisions with respect to their sensitivity to gauge boson coupling parameters. The processes are all of the general form

$$e^+e^- \to \ell^+\ell'^-\nu\bar{\nu}'. \tag{1.2}$$

Our work includes all possible charged lepton combinations, specifically $\mu\tau$, μe (τe), $\mu\mu$ ($\tau\tau$), and ee. The channels given in parentheses have the same set of Feynman diagram contributions as their corresponding unbracketed channel and we will henceforth drop reference to them as distinct processes.

In the next section, we describe the four types of processes with respect to their dependence on κ_V. We discuss our calculations in Sec. III and present results for the case of unpolarized beams. In Sec. IV, we present helicity amplitude information which is relevant to distinguishing κ_γ and κ_Z effects. Finally, we summarize our results.

II. FOUR LEPTON PROCESSES

In this section, we illustrate in detail the processes we are considering; in the diagrams of Figs. 1–7, the upper initial state fermion line is always the positron. We present separately first the Feynman diagram contributions which are κ_V dependent. The reactions (1.2) can all proceed via real or virtual W pair production, with the subsequent W decays into the appropriate leptonic modes. The form of the W pair production diagram which includes the triple gauge boson vertices is illustrated in Fig. 1. For the $\mu\tau$ final state, the diagrams of the type in Fig. 1 are the only ones with the γWW and ZWW vertices. The μe final state also receives contributions from two Feynman diagrams which contain the γWW and ZWW vertices, respectively, with a $\gamma(Z)$ and a W in the t channel; their form is shown in Fig. 2(a). Similarly, for the process $e^+e^- \to \mu^+\mu^-\nu\bar{\nu}$, there are two

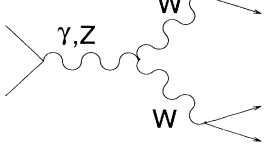

FIG. 1. The κ_V-dependent W pair production diagrams which are relevant to all the processes considered.

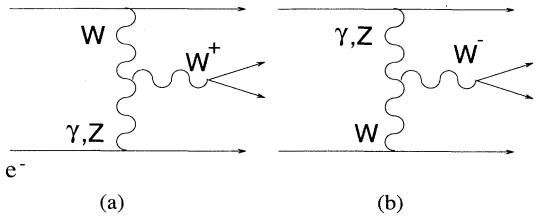

FIG. 2. The κ_V-dependent diagrams with one W and either a γ or Z in the t channel. (a) Contributes to the μ^+e^- and e^+e^- processes and (b) to the e^+e^- process.

diagrams containing the γWW and ZWW vertices, respectively, in addition to the W pair diagrams. The form of these contributions is shown in Fig. 3 and has the W bosons in the t channel coupling to a photon or Z which decays leptonically. Finally, all the diagrams containing the triple gauge boson vertices in Figs. 1, 2(a), and 3 contribute to the process $e^+e^- \to e^+e^-\nu\bar{\nu}$ as does the additional diagram of Fig. 2(b).

For all our processes, we include the full gauge invariant set of diagrams. The κ_V-independent diagrams are shown in Figs. 4–7. The first group, in Fig. 4, contributes to all the different final states. Figure 4(a) is just the usual t-channel neutrino exchange in W pair production. Figure 4(b) represents a set of diagrams; the s-channel Z boson in that diagram can produce either charged leptons or neutrinos and, for both the photon and Z diagrams, the W can be produced from either fermion leg, as the processes allow. The group of diagrams given in Fig. 5 contribute to the μ^+e^- and ee final states. Again, each of Figs. 5(a,b,c) represents a set of diagrams with various exchanged particles and with emission from the different initial and final fermions. The set of diagrams in Fig. 6 contributes to the final states with charged leptons of the same flavor, that is, to the $\mu\mu$ and ee cases. The diagrams of Fig. 7 contribute only to the ee final state. Note again that each diagram represents a set of possibilities; for example, in Fig. 7(b), the Z boson which decays to neutrinos can be emitted from any of the initial or final electrons or positrons.

Hence the $\mu^+\tau^-$ state can be produced via 9 different diagrams; the μ^+e^- state receives contributions from 18 diagrams. The $\mu\mu$ process has a total of 28 contributing diagrams with most of the extras being γ or Z "bremsstrahlung" from the initial or final state leptons. The ee process goes via 56 diagrams. For the $\mu\mu$ and ee final states, in some of the diagrams, all ν species can appear. These diagrams are added incoherently in the calculation. However, for the purpose of counting

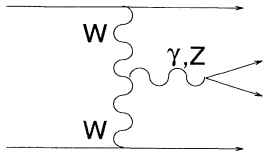

FIG. 3. The κ_V-dependent diagram with two W bosons in the t channel contributes to the $\mu^+\mu^-$ and e^+e^- processes.

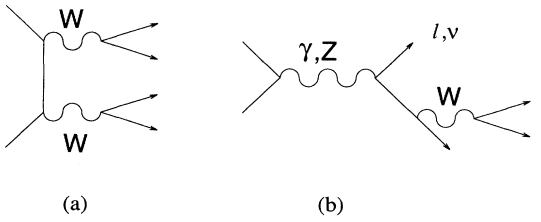

FIG. 4. The κ_V-independent diagrams which are relevant to all the processes considered.

the number of diagrams, we regard all the ν final states as contributing to a single diagram.

We can now make some points to justify the need for the full calculation that we present here as opposed to the calculations of W pair or single W production. At LEP II energies it is appropriate to calculate W pair production, the processes being dominated by the nearly on-shell W propagators. This is not the case, however, at higher energies unless one is dealing with a final state which allows for the experimental reconstruction of W's. We are considering here the purely leptonic final states. For this case, the W's can be reconstructed (up to a twofold ambiguity) only under the assumption that they are on shell [6]. We illustrate these points with the example of the calculation of the process $e^+e^- \to \mu^+e^-\nu_\mu\bar{\nu}_e$ at 500 GeV center-of-mass energy, subject to a variety of cuts on the invariant masses of the $\mu^+\nu_\mu$ and $e^-\bar{\nu}_e$ pairs, $M_{\mu\nu}$ and $M_{e\bar{\nu}}$, respectively. We postpone to the next section the description of the cuts we make motivated by detector considerations and background suppression and here note the results of imposing various cuts on invariant masses; these invariant mass cuts cannot be made experimentally for the leptonic states we consider. We calculate the μ^+e^- production with the cuts as follows:

$$\begin{aligned}
&(1)\ M_W - 5\ \text{GeV} \quad \le M_{\mu\nu} \le \quad M_W + 5\ \text{GeV},\\
&(2)\ M_W - 5\ \text{GeV} \quad \le M_{e\bar{\nu}} \le \quad M_W + 5\ \text{GeV},\\
&(3)\ M_W - 5\ \text{GeV} \le M_{\mu\nu},\ M_{e\bar{\nu}} \le M_W + 5\ \text{GeV}.
\end{aligned}$$

M_W is the W boson mass. The resulting cross sections, relative to that with no cut on the invariant masses, are in the ratio 1:0.84:0.54:0.44. The first cut, restricting the invariant mass of the $\mu^+\nu_\mu$ pair, includes W pair production, production of a single W^+ via the diagrams of Fig. 2(a), and production of nonresonant W^-'s. Cut

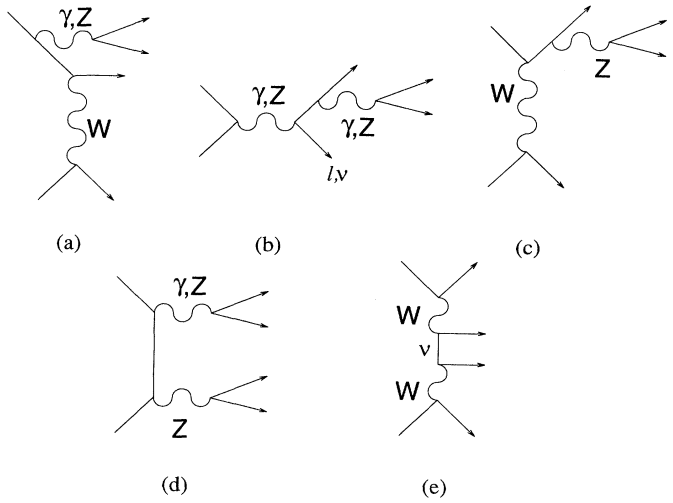

FIG. 6. The κ_V-independent diagrams which contribute to the $\mu^+\mu^-$ and e^+e^- processes.

(2), restricting only the $e^-\bar{\nu}_e$ invariant mass, reduces the cross section by a larger amount because there is no diagram equivalent to Fig. 2(a). (For the charge conjugate final state μ^-e^+, the role of the two cuts would be reversed.) Thus, this cut leaves W pair production along with nonresonant W^+'s. The third cut, where both the invariant masses are restricted, reduces to W pair production. Clearly, it is not sufficient to calculate only W pair production. Single W production is included in our calculation with the κ_V dependence illustrated in Fig. 2. Neither W pair nor single W production can be isolated by experimental cuts for the purely leptonic case. Consequently, we must fully calculate the $\ell^+\ell'^-\nu\bar{\nu}'$ production, as opposed to W pair production only and, in doing so, we aim to unearth a more realistic picture of the sensitivity to the couplings in question.

While discussing the set of four types of processes, we will also note here their helicity characteristics. In the following, we will denote the helicities of the particle set $e^+e^-\ell^+\ell'^-$ as $(\bar{\alpha}\alpha\bar{\beta}\beta)$. Figure 1 contributes to all the processes and goes via the helicity amplitudes $(+-+-)$ and $(-++-)$, and so each process we consider has these amplitudes. The $(+-+-)$ helicity is actually dominant in all cases. For the $\mu^+\tau^-$ final state, no other helicity amplitudes are introduced among the remaining seven

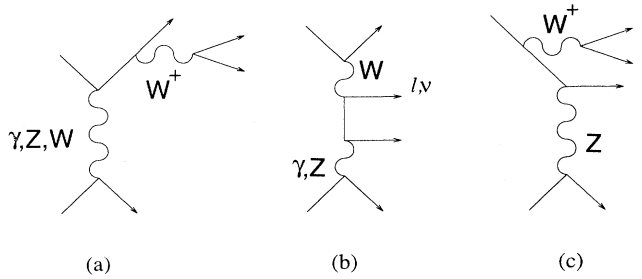

FIG. 5. The κ_V-independent diagrams which contribute to the μ^+e^- and e^+e^- processes.

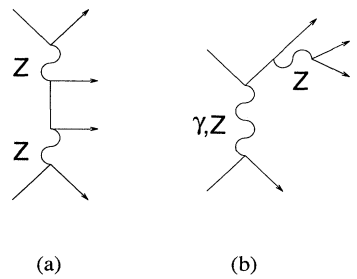

FIG. 7. The κ_V-independent diagrams which contribute to the e^+e^- process only.

diagrams. Figure 2(a) has contributions from $(+-+-)$ and $(+++-)$ helicity amplitudes; thus, the μ^+e^- final state has three helicity amplitudes contributing. For the $\mu^+\mu^-$ final state, the diagram of Fig. 3 contributes helicities $(+-+-)$ and $(+--+)$; in addition, some of the extra diagrams without the γWW or ZWW vertices have a $(-+-+)$ amplitude. Thus the $\mu^+\mu^-$ process has four helicity amplitudes; the $(-+-+)$ amplitude is independent of κ_γ and κ_Z. Figure 2(b) contributes $(+-+-)$ and $(----)$ amplitudes to the e^+e^- process. The e^+e^- process actually goes via all six possible helicity amplitudes; again, as in the $\mu^+\mu^-$ case, the $(-+-+)$ amplitude is κ_V independent, arising only in diagrams which do not contain the triple gauge boson vertices.

III. CALCULATIONS FOR UNPOLARIZED BEAMS

In order to deal easily with the large number of Feynman diagrams and to readily retain helicity information, we have written the amplitude for each process in the CALKUL helicity formulation [12]. We assume massless spinors describe the fermions although we do retain fermion masses in the propagators; this amounts to neglecting terms proportional to m_f, a good approximation. The matrix element squared for each process is embedded in a Monte Carlo algorithm for integration over the final state four-body phase space to yield the cross sections and various distributions. We sum and average over initial spins and sum over final spins. We use $M_Z = 91.196$ GeV, $\Gamma_Z = 2.534$ GeV, $M_W = 80.6$ GeV, $\Gamma_W = 2.25$ GeV, $m_e = 0.511$ MeV, $m_\mu = 0.1057$ GeV, $m_\tau = 1.7841$ GeV, and $\sin^2\theta_W = 0.23$.

We have performed a number of checks on our calculations. We have checked our algorithms by showing that our $\mu\tau$ results reduce to those of W pair production [6,13] if only the appropriate contributions are included; this included checking that the individual contributions from the three W pair diagrams, $M_{\gamma\gamma}$, M_{ZZ}, and $M_{\nu\nu}$, and those from their interferences, $M_{\gamma Z}$, $M_{\gamma\nu}$, and $M_{\nu Z}$, were reproduced properly. Another useful check on our matrix elements is that of charge conjugation; we generated various redundant distributions for the positively and negatively charged leptons for the $\mu^+\mu^-$, e^+e^-, and $\mu^+\tau^-$ (invariant up to the μ τ mass difference) channels as a check. In addition, we generated a number of distributions which are not actually experimentally observable for our processes due to the two neutrinos, such as the angular and invariant mass distributions of the reconstructed W bosons in order to note their consistency with W pair production work [6,13].

The experimental signature for the processes under consideration is a clean one, an oppositely charged lepton pair and missing transverse momentum and energy due to the neutrinos. We have made some fairly simple cuts as described below to account for detector acceptance and potential backgrounds. For all the processes, we require a cut on the angle of each of the charged leptons relative to the beam such that $-0.95 \leq \cos\theta_{\ell\pm} \leq 0.95$. This is the only cut we impose for the $\mu\tau$ and μe final states. This angular cut is experimentally motivated; however, it also serves to regulate the t-channel photon pole from the diagrams of Figs. 2(a,b) allowing us to neglect the terms proportional to m_f. These diagrams contribute to the μ^+e^- and e^+e^- final states, as described above.

One potential background is τ pair production with each of the τ's decaying leptonically. At $\sqrt{s}$ of 200 GeV, each of the four lepton processes and the τ pair production, multiplied by the branching ratios of τ into e or μ of 17.8% each [14], yield about the same rate. At higher energies, the τ pair production cross section is falling like $1/s$ while the cross section for our processes remains large. In addition, the τ pair process should have substantially greater missing energy with four neutrinos in the final state. It seems that this source of background is manageable.

The four lepton processes with one or more τ's in the final state ($\mu\tau$ and $\tau\tau$) could feed down as a background to the processes without any τ if the τ('s) decays leptonically. However, factoring in the τ decay branching ratio and accounting for the higher missing energy keep this background under control.

Another potential background comes from two photon processes with the e^+ and e^- undetected near the beam. This is relevant to the $\mu\mu$ and ee processes and we make a cut on missing transverse momentum to eliminate two photon events as a background source; we require total visible $p_T > 10$ GeV. We also require for these two processes that each charged lepton carry a minimum energy, $E_\ell > 10$ GeV. Finally, again for the $\mu\mu$ and ee processes we make a cut on the invariant mass of the charged lepton pair; we require $m_{\ell^+\ell^-} > 25$ GeV in order to eliminate the low invariant mass dileptons corresponding to the photon pole in these processes.

In Figs. 8(a,b,c,d), we show the cross sections as a function of $\sqrt{s}$ for the processes $e^+e^- \to \ell^+\ell'^-\nu\bar{\nu}'$ for $\ell^+\ell'^-$ equal to $\mu^+\tau^-$, μ^+e^-, $\mu^+\mu^-$, e^+e^-, respectively, with the cuts as described above imposed. In each case, the solid line corresponds to the case of standard model couplings, $\kappa_\gamma = \kappa_Z = 1$, while the dashed line is for $\kappa_\gamma = \kappa_Z = 0.9$, an example of a 10% deviation with the couplings set equal. The sensitivity to κ_V increases with increasing center-of-mass energy. The $\mu\tau$ process exhibits the most sensitivity to κ_V, as might be expected since it has the least number of extraneous contributing diagrams; however, it also has the smallest cross section. Thus, it is useful to consider all the processes.

We make our study of κ_V dependence at two center-of-mass energies, 500 GeV and 1 TeV, motivated by the possibility of future high energy e^+e^- colliders. For each of the four types of four lepton processes, at each of the two energies, we vary κ_γ alone from 0.9 to 1.1, κ_Z alone over the same range, and κ_γ constrained to equal κ_Z over the same range. As an example, we show the ratio of the cross section with nonstandard couplings to the standard model cross section for the $\mu^+\tau^-$ process at $\sqrt{s}$ of 500 GeV and 1 TeV in Figs. 9(a) and 9(b), respectively; in each case, the solid line corresponds to κ_γ set equal to κ_Z, the dashed line to $\kappa_Z = 1$, and the dotted line to $\kappa_\gamma = 1$. For reference, the standard model cross section in this case is 0.034 pb at $\sqrt{s}$ of 500 GeV and 0.009 pb at $\sqrt{s}$

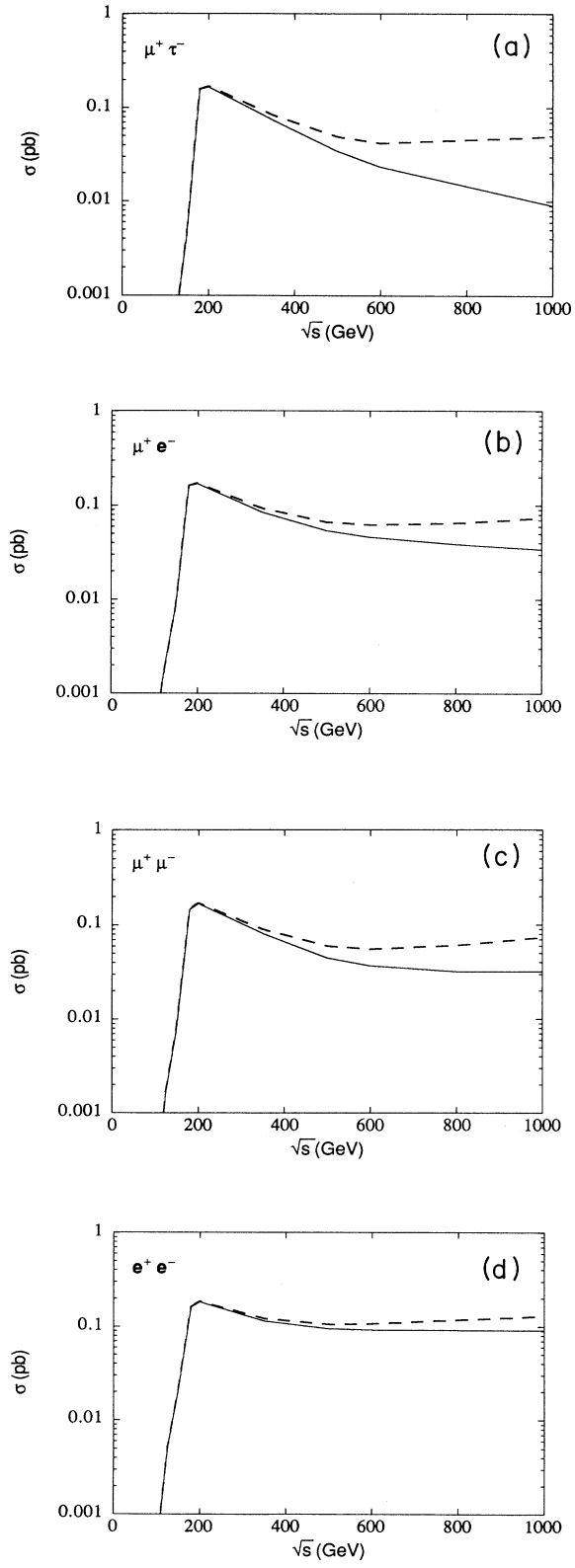

FIG. 8. The total cross section as a function of center-of-mass energy for the (a) $\mu^+\tau^-$, (b) μ^+e^-, (c) $\mu^+\mu^-$, and (d) e^+e^- processes. The solid line in each figure corresponds to the standard model case while the dashed lines are for $\kappa_\gamma = \kappa_Z = 0.9$.

of 1 TeV. As in this example, we find that the $\kappa_\gamma = \kappa_Z$ case always shows the greatest deviation from the standard model value of the cross section. At $\sqrt{s}$ of 500 GeV, each process is more sensitive to deviations of κ_V below the standard model value of 1 than above it; however, at the higher center-of-mass energy of 1 TeV, the sensitivity to κ_V is considerably more symmetric about 1. Varying either κ_γ or κ_Z separately or setting them equal, the amplitude at each energy for each process can be expressed as $M = \alpha + \beta\kappa$; we have in each case fit a parabola for the cross section as a function of κ and solved for the cross section as a function of the two parameters κ_γ and κ_Z as

$$\sigma \sim |M|^2 = a + b\kappa_\gamma + c\kappa_Z + d\kappa_\gamma\kappa_Z + e\kappa_\gamma^2 + f\kappa_Z^2. \tag{3.1}$$

In Figs. 10(a,b,c,d), we show the resulting surface plots of the cross sections for the $\mu\tau$, μe, $\mu\mu$, and ee processes, respectively, as a function of κ_γ and κ_Z at $\sqrt{s}$ of 500 GeV. The corresponding results for $\sqrt{s}$ of 1 TeV are given in Figs. 11(a–d). We have checked that a run over a grid of various $(\kappa_\gamma, \kappa_Z)$ values reproduces these results.

We turn these results into limits on the detection of deviations of κ_V from 1 by assuming an integrated luminosity of 50 fb^{-1} for a proposed collider [15]. Figures

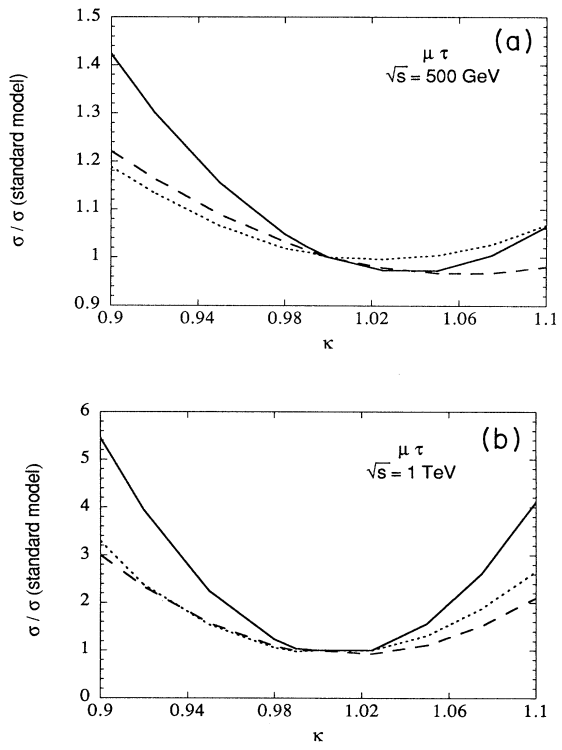

FIG. 9. For the $\mu\tau$ process at (a) 500 GeV and (b) 1 TeV, the ratio of the cross section for nonstandard values of κ_V to the standard model cross section as a function of κ_V. The solid line corresponds to $\kappa_\gamma = \kappa_Z$, the dashed line to $\kappa_Z = 1$, and the dotted line to $\kappa_\gamma = 1$ in parts (a) and (b).

12(a,b,c,d) are 1σ and 2σ contour plots for the $\mu\tau$, μe, $\mu\mu$, and ee processes, respectively, at 500 GeV center-of-mass energy. The solid lines on each plot are the 1σ contours and the dashed lines are the 2σ contours, with statistical errors only included. The corresponding contours for $\sqrt{s} = 1$ TeV are given in Figs. 13(a–d). In obtaining these results, we have included a factor of 2 to account for the charge conjugate processes in the $\mu^+\tau^-$ ($\mu^-\tau^+$) and μ^+e^- (μ^-e^+) channels. The τe and $\tau\tau$ channels would yield results as for the μe and $\mu\mu$ channels, respectively, the μ τ mass difference being negligible here. Thus, from the total cross section of the individual processes, we find the following 2σ limits on measurements of κ_γ and κ_Z. At $\sqrt{s}$ of 500 GeV, κ_γ could be measured within -2.5% ($\mu\tau$) to $+9.5\%$ (ee) and κ_Z within the range -6% ($\mu\tau$, μe, $\mu\mu$) to $+8\%$ (μe). At 1 TeV, the corresponding limits on κ_γ are -1% ($\mu\tau$) to $+3.5\%$ ($\mu\tau$, μe) and on κ_Z we find limits of -1.5% ($\mu\tau$) to $+2.5\%$ ($\mu\tau$). The channels given in parentheses with each limit indicate which of the processes supplies the best bound. These particular limits simply represent the outer bound of the 2σ contour for the various processes. If one makes some assumptions about the relationship of κ_γ and κ_Z, such as that $\kappa_\gamma = \kappa_Z$ or that $\Delta\kappa_\gamma = \frac{2\cos^2\theta_W}{\cos^2\theta_W - \sin^2\theta_W}\Delta\kappa_Z$ [5], better bounds (which can be read off Figs. 12 and 13) are obtained. In addition, combining the statistics from all the processes considered here would improve the bounds. In fact, one could also combine these four lepton processes with the similar jet channels such as $e^+e^- \to q\bar{q}'\ell\nu$. Combined bounds would necessitate inclusion of detector acceptances and efficiencies for the various particle types.

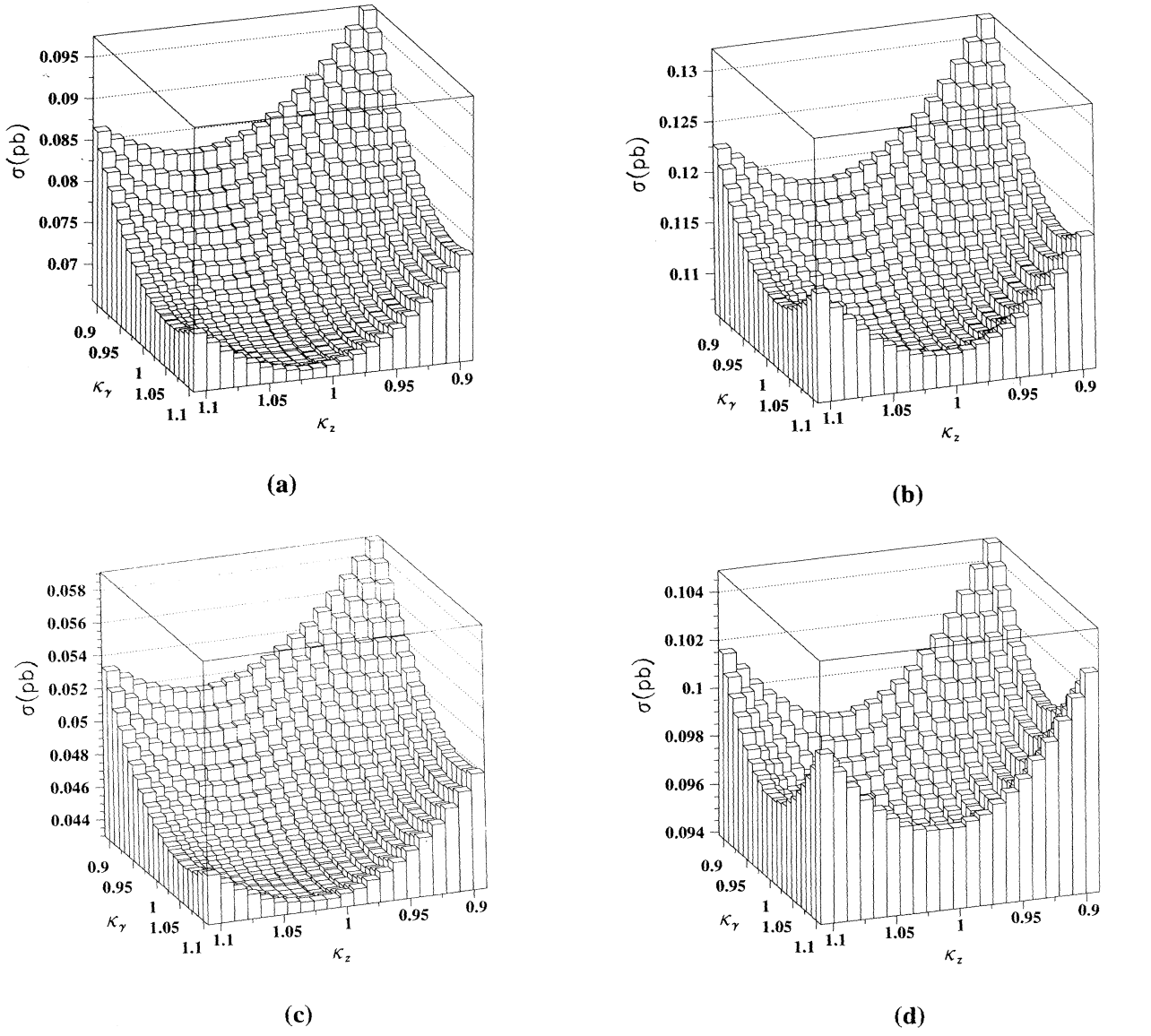

FIG. 10. At the center-of-mass energy of 500 GeV, the cross section as a function of κ_γ and κ_Z for the (a) $\mu\tau$, (b) μe, (c) $\mu\mu$, and (d) ee processes.

We emphasize that even the bounds quoted above from the cross sections of individual processes are, indeed, approaching the very interesting realm of probing κ_V to within a few percent of the standard model value. We note that it is particularly important to go to the higher energy in order to probe values of κ_V larger than 1.

We have also generated a number of distributions; these include the differential cross sections with respect to the angle of each charged lepton relative to the beam, the angle between the charged leptons, the energy and transverse momentum of each charged lepton, the total visible energy and transverse momentum, and the invariant mass of the charged lepton pair. The charged lepton angular distributions tend to be strongly peaked along the beam line due to the t-channel neutrino exchange; they are generally enhanced somewhat away from the beam direction for nonstandard κ_V values. The energy and transverse momentum distributions of the individual particles tend to be enhanced over most of their range. The total visible transverse momentum is preferentially enhanced where the differential cross section is largest. As examples, we show in Figs. 14(a) and 14(b) the differential cross section with respect to the total visible transverse momentum for the $\mu\tau$ and $\mu\mu$ processes, respectively, both at a center-of-mass energy of 500 GeV. The solid line in each figure represents standard model couplings and the dotted line is for the case of $\kappa_\gamma = \kappa_Z = 0.9$. The differential cross section with respect to x_-, where $x_- = E_-/(\sqrt{s}/2)$, is shown in Figs. 15(a) and 15(b) for the same two processes. E_- is the energy of the neg-

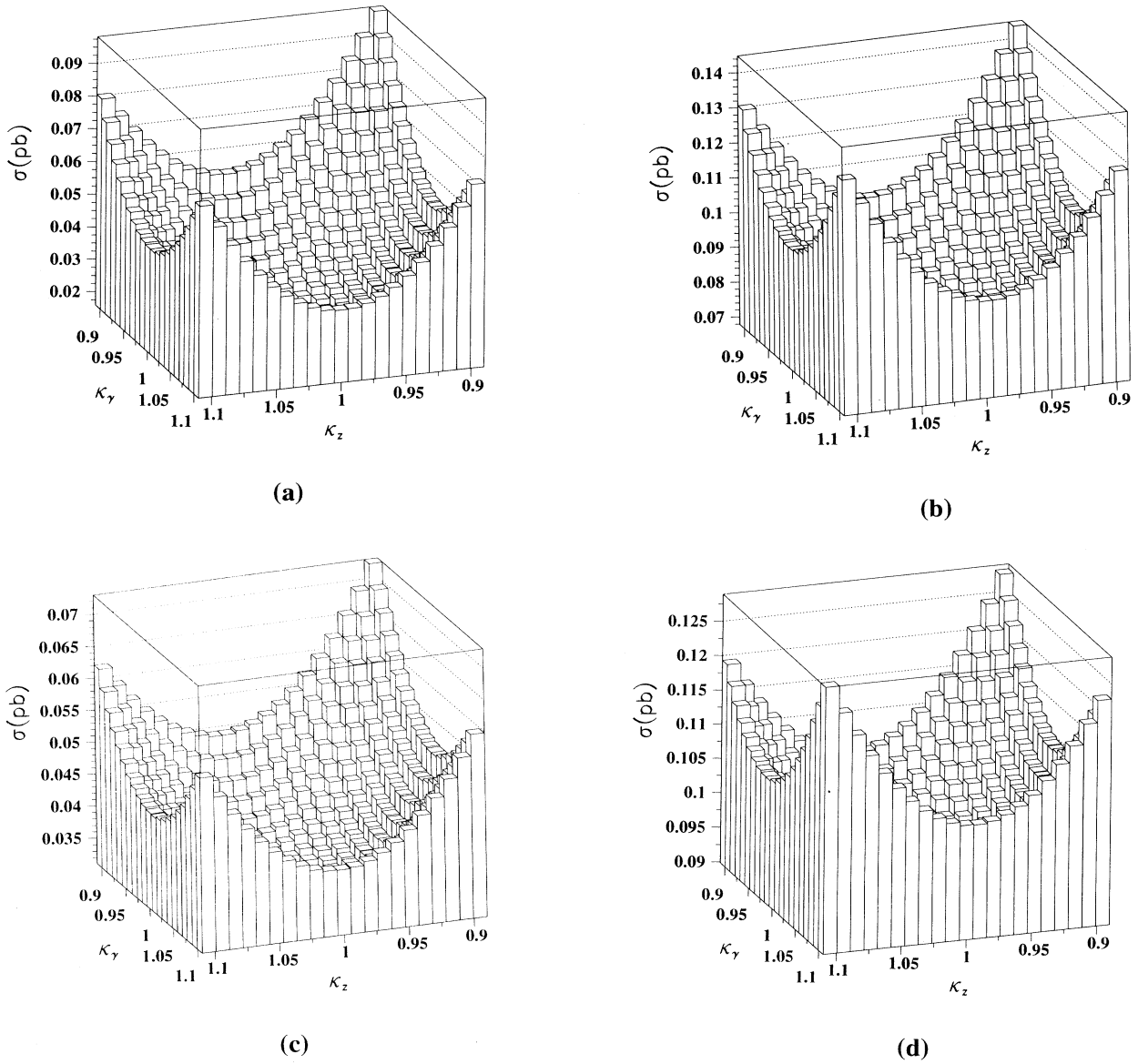

FIG. 11. At the center-of-mass energy of 1 TeV, the cross section as a function of κ_γ and κ_Z for the (a) $\mu\tau$, (b) μe, (c) $\mu\mu$, and (d) ee processes.

atively charged final state lepton. The notation is the same as for Fig. 14.

The potential for enhancing the κ sensitivity with cuts on some of these variables exists and we have made some preliminary investigations. There is a great deal of information within the distributions, beyond what is gained from the total cross section measurements alone. We indicate some of this detail with the results of a couple of cuts for the μe process at 500 GeV for the case of $\kappa_\gamma = \kappa_Z$. For this case, with our standard cuts as described above, we found sensitivity to the $\Delta\kappa$ range -2.7%–7%. The effect of making a stronger cut on the charged lepton angles such that $\cos\theta_e \geq -0.7$ and $\cos\theta_\mu \leq 0.7$, in order to cut out the peaking along the beam direction, is to improve the sensitivity for κ less than 1 from -2.7% to -1.1%. However, for κ above 1, the sensitivity is actually slightly degraded to 7.5%. This happens because we have κ sensitivity in the peak region; along with the κ-independent t-channel neutrino diagram, there is also the κ-dependent t-channel photon diagram. For concreteness, we can discuss two κ sets that have approximately the same total cross section, with one set below and one above the standard model value of 1, $\kappa = 0.95$ and $\kappa = 1.09$. In the peaked part of the angular distributions, the $\kappa = 0.95$ rate is very close to and slightly below the standard model rate while the $\kappa = 1.09$ rate is enhanced above the standard model throughout the entire angular range. Away from the peaked region, the $\kappa = 0.95$ rate grows larger than the $\kappa = 1.09$ rate and both are above the standard model. Hence, cutting out

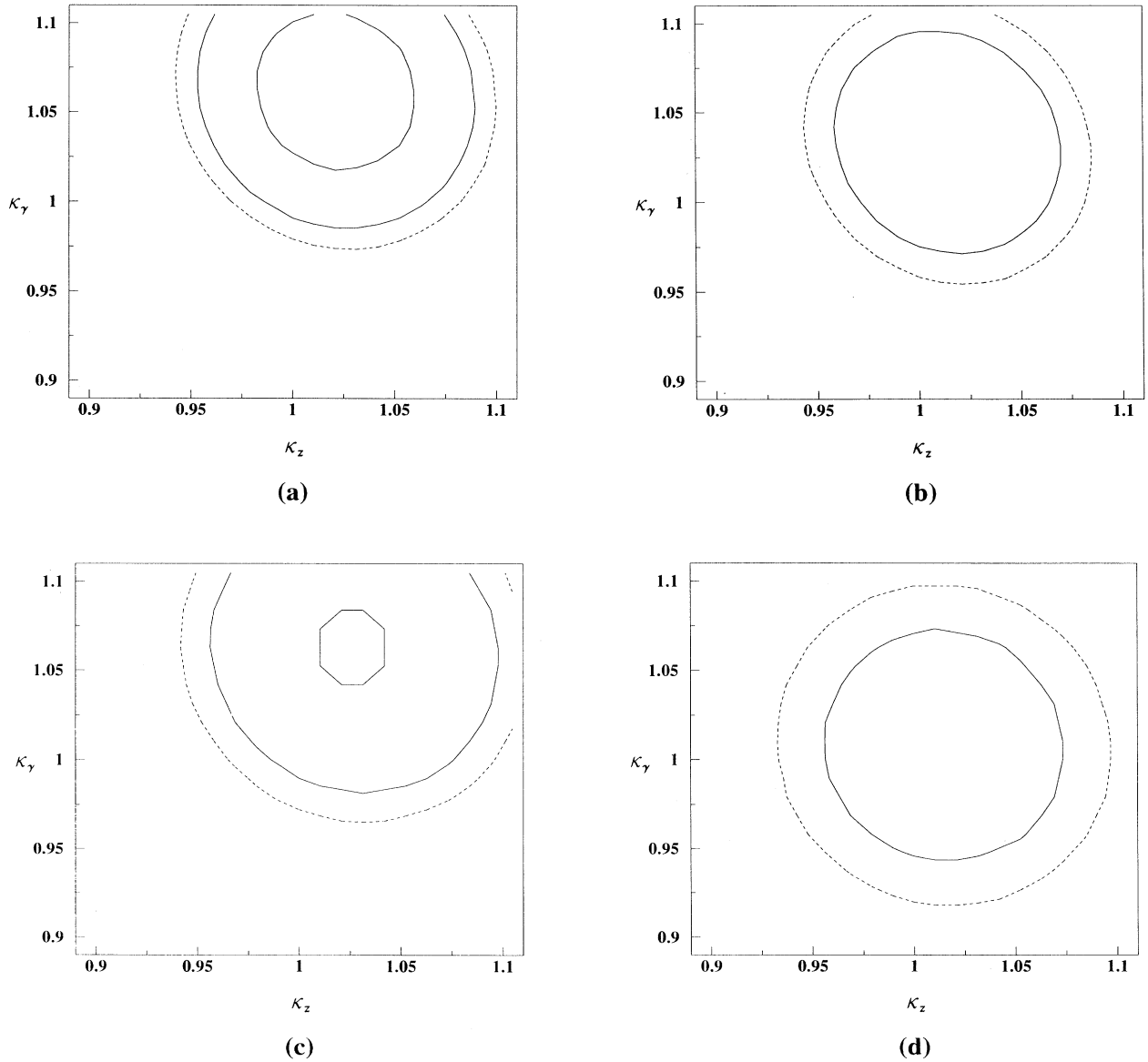

FIG. 12. Contour plots in κ_γ and κ_Z at the 1σ (solid lines) and 2σ (dashed lines) levels for the (a) $\mu\tau$, (b) μe, (c) $\mu\mu$, and (d) ee processes at 500 GeV.

the peak area does improve the sensitivity for $\kappa = 0.95$ (or, more generally, for κ below 1), but it does not for the $\kappa = 1.09$ (κ above 1) case because there is some sensitivity within that (high statistics) part of the spectrum that one is cutting out. Another cut which we tried was in the invariant mass of the charged lepton pair such that 90 GeV$\leq M_{\mu e} \leq$350 GeV. That cut, in combination with our standard angular cuts, made a very slight improvement in the κ sensitivity for κ below 1; in combination with the stronger angular cuts described above, the κ sensitivity improved to -1% for κ below 1.

We can conclude that one can generally expect to improve the sensitivity to κ values below 1 by about 1% or so with various cuts. It seems more difficult to improve the sensitivity for κ above 1 because the enhancement above the standard model tends to be spread more uniformly over the range of the variables which we considered. Definitive assessments of the usefulness of cuts depend greatly on the actual κ values; the cuts ultimately need to be tailored for the specific experimental distributions when compared with the standard model expectations.

IV. HELICITY CONSIDERATIONS

Referring to the three-dimensional plots of Figs. 10(a–d) and 11(a–d), note that a plane of constant cross section intersects a ring of $(\kappa_\gamma, \kappa_Z)$ pairs. So we can apparently determine, within the limits given in the last section, a deviation from the standard model with cross sec-

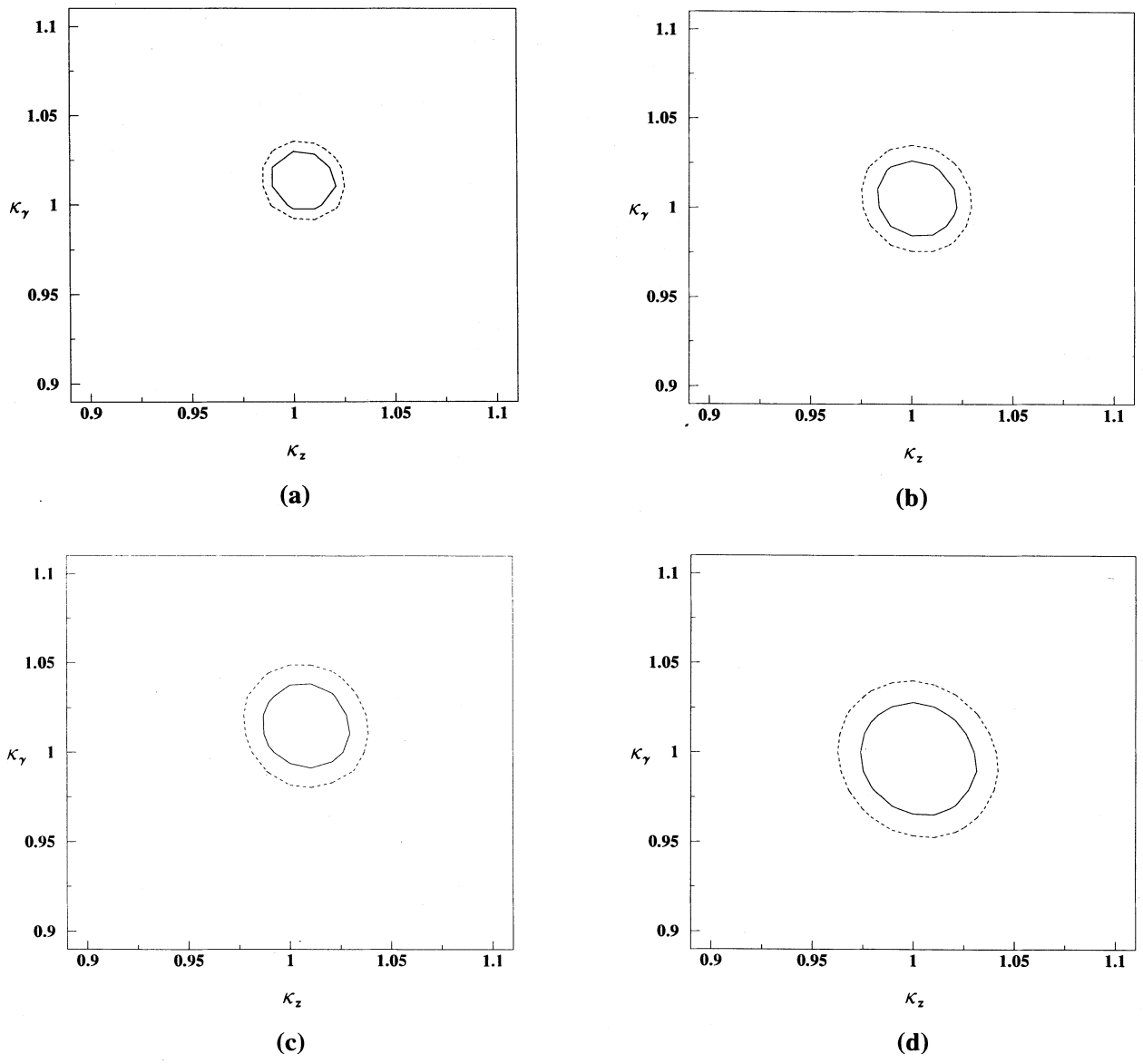

FIG. 13. Contour plots in κ_γ and κ_Z at the 1σ (solid lines) and 2σ (dashed lines) levels for the (a) $\mu\tau$, (b) μe, (c) $\mu\mu$, and (d) ee processes at 1 TeV.

tion measurements, but it remains to determine whether we can pinpoint the values of κ_γ and κ_Z individually. There have been a number of approaches proposed for discriminating between deviations of κ_γ and κ_Z. One suggestion is to study processes which only involve one or the other of the γWW and ZWW vertices. The associated production of a W with either a γ or a Z boson, radiative W decay [16], and $e\gamma$ processes such as $e\gamma \to W\nu$ [17] fall into this category. Another suggestion is to make cuts which isolate one of the vertices. For instance, Couture, Godfrey, and Lewis have studied the $\mu^+\mu^-$ production process which we also consider here and have focused on the ZWW vertex by requiring that the invariant mass of the $\mu^+\mu^-$ pair fall within 5 GeV of M_Z [18]. This, in effect, helps to isolate the Z contribution from the diagram of the form of Fig. 3.

Here, we emphasize instead the potential usefulness of the helicity structure in providing a determination of κ_γ and κ_Z. For instance, we can make one general statement regarding the contribution to the total unpolarized cross section of the $(-++-)$ helicity. Recall that this amplitude contributes to all our processes since it occurs for the W-pair-type diagrams of Fig. 1, although it is not the dominant amplitude. [As previously noted, $(+--+)$ is the dominant amplitude.] We observe that the $(-++-)$ amplitude is suppressed at $\sqrt{s} \gg M_Z$ for $\kappa_\gamma = \kappa_Z$ as a direct result of the general form of this amplitude, which is given below:

$$M_{(-++-)} = \left[\frac{\kappa_\gamma + 1}{2s} - \frac{\kappa_Z + 1}{2(s - M_Z^2)}\right] A + B. \qquad (4.1)$$

Here A and B denote the κ_V-dependent and -independent factors, respectively, of the amplitude. For large center-of-mass energies, the cancellation of the κ_γ and κ_Z terms results in a $(-++-)$ helicity contribution of less than about 1% of the total cross section for the standard model and for $\kappa_\gamma = \kappa_Z$ in general. On the other hand, for nonequal values of κ_γ and κ_Z, this contribution can be as much as 30% of the total. In Fig. 16, we illustrate this general behavior with examples for the $\mu\tau$ process. In this process, only two helicity amplitudes contribute, and so presentation is simplified, although the suppression of the $(-++-)$ is general for all the processes as described above. We display the differential cross section with respect to total visible transverse momentum for three sets of $(\kappa_\gamma, \kappa_Z)$ values. Figures 16(a,b,c) represent (1.0,1.0), (0.9,1.0), and (0.9,0.9), respectively, at $\sqrt{s}$ of 1 TeV. The solid line corresponds to the unpolarized cross section, the dashed line to the $(+-+-)$ helicity contribution, and the dotted to the $(-++-)$ contribution. The $(-++-)$ amplitude is enhanced in Fig. 16(b), where κ_γ is not equal to κ_Z. Thus, polarized beams accessing the individual helicity contributions could differentiate between the $\kappa_\gamma = \kappa_Z$ case and the nonequal case.

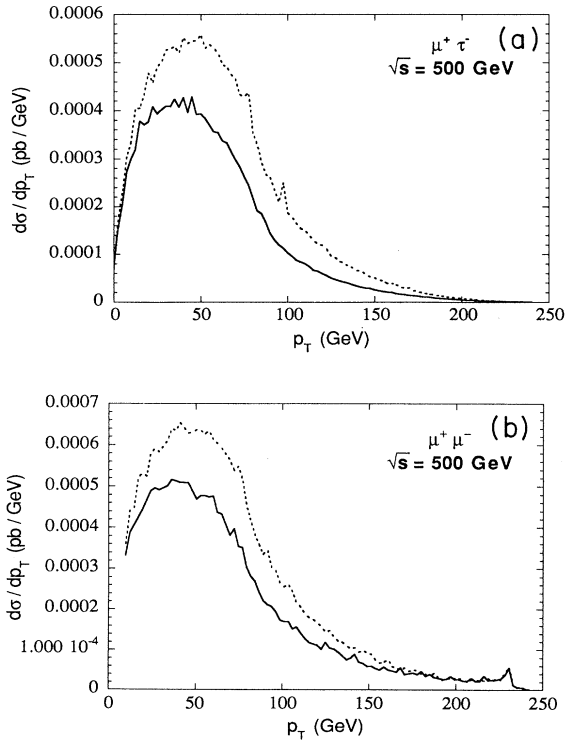

FIG. 14. The differential cross section with respect to total visible transverse momentum at a center-of-mass energy of 500 GeV for the (a) $\mu\tau$ and (b) $\mu\mu$ processes. The solid line corresponds to the standard model while the dotted line is for $\kappa_\gamma = \kappa_Z = 0.9$.

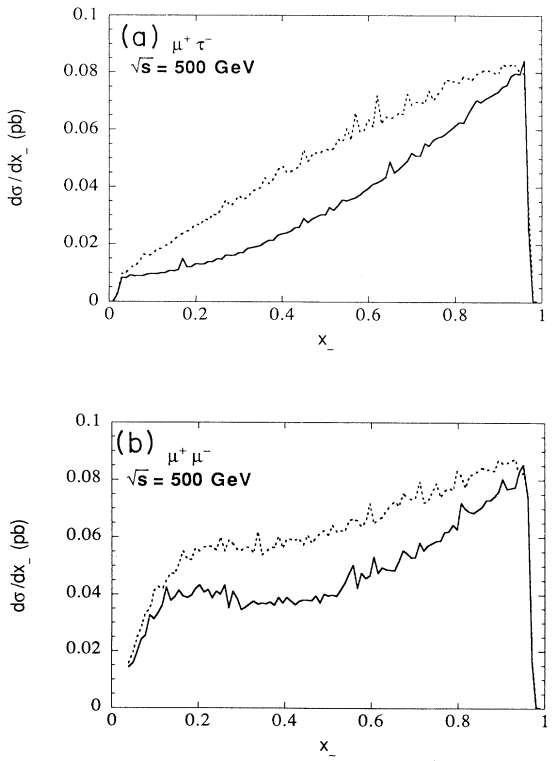

FIG. 15. The differential cross section with respect to the normalized energy variable of the negative lepton, x_-, at a center-of-mass energy of 500 GeV for the (a) $\mu\tau$ and (b) $\mu\mu$ processes. The solid line corresponds to the standard model while the dotted line is for $\kappa_\gamma = \kappa_Z = 0.9$.

Apart from the general observation described above regarding the case of κ_γ and κ_Z equal, experimental results on the cross sections for the four types of processes we consider with polarized and unpolarized beams could provide a characteristic "fingerprint" for a $(\kappa_\gamma, \kappa_Z)$ pair. As an example of how this might work, refer to Fig. 9 for the $\mu\tau$ process at 1 TeV; from that plot, we note that, for instance, $(\kappa_\gamma, \kappa_Z)$ =(0.945,0.945), (1.07,1.07), (1,1.095), (1,0.92), and $(0.92, 1)$ all have approximately the same total cross section. The percentage of the cross section supplied by the $(-++-)$ helicity is less than 1% for the two cases quoted with $\kappa_\gamma = \kappa_Z$; it is 3.6% for $(1, 1.095)$, 18% for $(1, 0.92)$, and 27% for $(0.92, 1)$. Since the total cross section for unpolarized beams corresponds to about 1000 events, these cases can possibly be discriminated providing reasonable polarization can be achieved. In Fig. 17, we illustrate, for the $\mu\tau$ process at 1 TeV, the $(+-+-)$ and $(-++-)$ helicity contributions to the differential cross section with respect to the normalized τ energy, x_-, for $(\kappa_\gamma, \kappa_Z) = (0.945, 0.945)$ (solid lines), $(1, 0.92)$ (dashed lines), and $(0.92, 1)$ (dotted lines). In each case, the $(+-+-)$ helicity is the larger of the two corresponding contributions and so is the upper line in each pair. For the $(\kappa_\gamma, \kappa_Z) = (0.945, 0.945)$ case, the $(-++-)$ contribution is very small relative to the scale of the figure, and so it is marked also with diamonds. The figure indicates the relative contribution from the different helicities for the various values of κ_V. For simplicity of presentation, we do not show the sum of the amplitudes but point out here that not only are the total cross sections very similar for the various $(\kappa_\gamma, \kappa_Z)$ pairs but, in fact, the distributions for unpolarized beams are as well; it is only for the various individual polarization contributions that the $(\kappa_\gamma, \kappa_Z)$ sets are distinguished. Similar results from the four types of processes can be combined to narrow in on the actual values of κ_γ and κ_Z, individually. A detailed study of distributions will also be useful as mentioned in the last section.

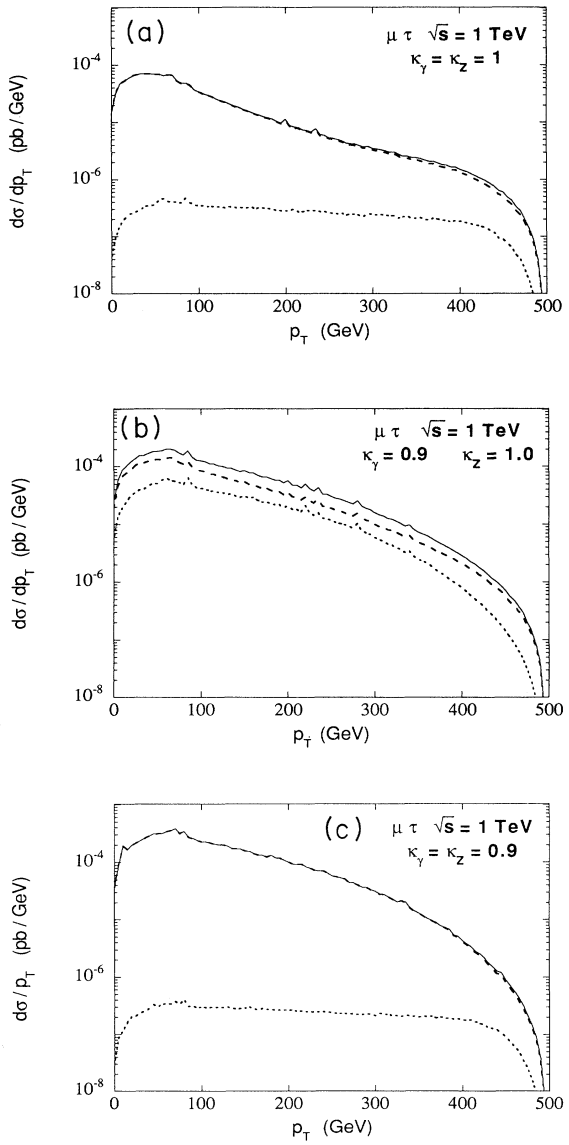

FIG. 16. For the $\mu\tau$ process at the center-of-mass energy of 1 TeV, the differential cross section with respect to the total visible transverse momentum for (a) $\kappa_\gamma = \kappa_Z = 1$, (b) $\kappa_\gamma = \kappa_Z = 0.9$, and (c) $\kappa_\gamma = 0.9$ with $\kappa_Z = 1$. The solid line is the sum of all helicity amplitude contributions, the dashed line is the $(+-+-)$ contribution, and the dotted line is the $(-++-)$ contribution.

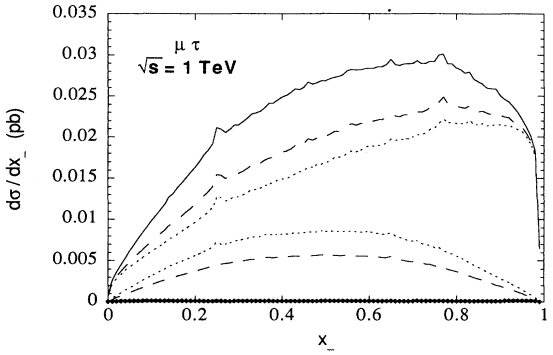

FIG. 17. For the $\mu\tau$ process at 1 TeV, the $(+-+-)$ and $(-++-)$ contributions to the differential cross section with respect to the normalized τ energy, x_-, for $(\kappa_\gamma, \kappa_Z) = (0.945, 0.945)$ (solid lines), (1,0.92) (dashed lines), and (0.92,1) (dotted lines). In each pair of lines, the upper line represents the dominant $(+-+-)$ contribution; for the (0.945,0.945) case, the $(-++-)$ contribution is very small on the scale of the figure and is marked with diamonds.

V. SUMMARY AND CONCLUSIONS

We have presented a study of the sensitivity to W boson coupling parameters κ_γ and κ_Z of the process $e^+e^- \to \ell^+\ell'^-\nu\bar{\nu}'$, including the charged lepton final states $\mu\tau$, μe (τe), $\mu\mu$ $(\tau\tau)$, and ee. The full matrix element calculation has been performed for each of the four types of processes. We find that, for a 500 GeV e^+e^- collider achieving an integrated luminosity of 50 fb^{-1}, κ_γ could be measured within the limits from 0.975 to 1.095 at the 2σ level and κ_Z within the limits 0.94 to

1.08. For a 1 TeV collider with the same luminosity, the corresponding limits are from 0.99 to 1.035 for κ_γ and from 0.985 to 1.025 for κ_Z. These limits are all for total cross section measurements of individual reactions and can be improved somewhat with the judicious choice of cuts. The 1 TeV limits, in particular, are very interesting even at the level of standard model radiative corrections; the higher energy is particularly important in determining κ_V values which may be greater than the standard model tree level value of 1.

We have also found that beam polarization would be useful in determining values of κ_γ and κ_Z individually as opposed to merely a deviation of either parameter from the standard model value. For all the processes, the helicity amplitude $(-++-)$ is suppressed in the case that κ_γ and κ_Z are equal at the high energies considered here. Thus, for instance, if the dominant $(+-+-)$ helicity contributed within about 1% of the total cross section for the $\mu\tau$ process, equality of κ_γ and κ_Z would be indicated. On the other hand, for nonequal values, the $(+-+-)$ contribution might be as little as 70%. Thus, polarized beams could determine the contributions of the various helicity amplitudes and yield values of κ_γ and κ_Z individually.

In conclusion, the processes considered here offer a very clean experimental signature for excellent sensitivity to κ_γ and κ_Z at a high energy e^+e^- collider.

ACKNOWLEDGMENTS

This work was funded in part by the Natural Sciences and Engineering Council of Canada. P.K. gratefully acknowledges the hospitality of the Phenomenology Institute at the University of Wisconsin at Madison and useful discussions with Dieter Zeppenfeld. The authors also thank Stephen Godfrey for helpful discussions.

[1] M. Timko, presented at the Spring Meeting of the American Physical Society, Washington, D.C., 1990 (unpublished).
[2] J. Alitti *et al.*, Phys. Lett. B **277**, 194 (1992).
[3] A. De Rújula *et al.*, Nucl. Phys. **B384**, 3 (1992); D. Choudhury, P. Roy, and R. Sinha, Report No. TIFR-TH/93-08 (unpublished).
[4] C. Burgess and D. London, Phys. Rev. D **48**, 4337 (1993); Phys. Rev. Lett. **69**, 3428 (1992).
[5] K. Hagiwara *et al.*, Phys. Lett. B **283**, 353 (1992).
[6] K. Hagiwara *et al.*, Nucl. Phys. **B282**, 253 (1987).
[7] J.F. Gaemers and G.J. Gounaris, Z. Phys. C **1**, 259 (1979).
[8] W. Marciano and A. Queijeiro, Phys. Rev. D **33**, 3449 (1986); F. Boudjema *et al.*, *ibid.* **43**, 2223 (1991).
[9] T.G. Rizzo and M.A. Samuel, Phys. Rev. D **35**, 403 (1987).
[10] G. Couture *et al.*, Phys. Rev. D **36**, 859 (1987).
[11] G. Couture *et al.*, Phys. Rev. D **38**, 860 (1988).
[12] R. Kleiss and W.J. Stirling, Nucl. Phys. **B262**, 235 (1985).
[13] F. Bletzacker and H.T. Nieh, Nucl. Phys. **B124**, 511 (1977); P. Mery and M. Perrottet, *ibid.* **B175**, 234 (1980); C.L. Bilchak and J.D. Stroughair, Phys. Rev. D **30**, 1881 (1984).
[14] M. Aguilar-Benitez *et al.*, Phys. Rev. D **45**, 4365 (1992).
[15] This estimated integrated luminosity is based on information in *Proceedings of the Third Workshop on the Japan Linear Collider*, Tsukuba, Japan, 1991, edited by A. Miyamoto (KEK Report No. 91-10, Tsukuba, 1991); Search for New Phenomena at Colliding Beam Facilities, Proceedings, New Haven, Connecticut, 1992 (in press).
[16] K.O. Mikaelian, M.A. Samuel, and D. Sahdev, Phys. Rev. Lett. **43**, 746 (1979); J. Cortes, K. Hagiwara, and F. Herzog, Nucl. Phys. **B278**, 16 (1986); U. Baur and D. Zeppenfeld, *ibid.* **B308**, 127 (1988); U. Baur and E. Berger, Phys. Rev. D **41**, 1476 (1990); M. Samuel *et al.*, Phys. Lett. B **280**, 124 (1992).
[17] G. Couture, S. Godfrey, and P. Kalyniak, Phys. Lett. B **218**, 361 (1989); Phys. Rev. D **39**, 3239 (1989); **42**, 1841 (1990).
[18] G. Couture, S. Godfrey, and R. Lewis, Phys. Rev. D **45**, 777 (1992).